NASA TN D-424

TECHNICAL NOTE
D-424

INVESTIGATION OF THE BUCKLING STRENGTH OF CORRUGATED WEBS IN SHEAR

By James P. Peterson and Michael F. Card

Langley Research Center
Langley Field, Va.

NATIONAL AERONAUTICS AND SPACE ADMINISTRATION

WASHINGTON

June 1960

NATIONAL AERONAUTICS AND SPACE ADMINISTRATION

TECHNICAL NOTE D-424

INVESTIGATION OF THE BUCKLING STRENGTH OF CORRUGATED WEBS IN SHEAR

By James P. Peterson and Michael F. Card

SUMMARY

Design charts are presented from which the buckling strength of corrugated shear webs can be determined. The charts are applicable to webs with supported edges in which the edge rotations of the web along lines of support may range from unrestrained (simply supported edges) to completely restrained (clamped edges). In addition, the results of shear tests on seven beams with corrugated webs are presented and discussed.

INTRODUCTION

The geometric properties of corrugated sheet adapt it particularly well to certain structural applications, one of the more important of which is the shear web. Corrugated sheet has been recognized for some time as an effective medium for transmitting shear loads (see, for instance, ref. 1), but it has not been generally used for this purpose because of certain inherent difficulties associated with fabrication and stress analysis. More recently, however, corrugated webs have been considered in structural applications where the webs are required to perform dual functions. For instance, corrugated webs may be used in high-temperature environment applications for their thermal stress-alleviating properties as well as for their shear-carrying properties, or they may be used in a sandwich-covered wing structure where fewer webs than usual are employed and where each web is required to possess a relatively large crushing strength as well as a large shear buckling strength.

The design information available is generally inadequate to predict the buckling behavior of corrugated shear webs. Buckling charts are available for orthotropic plates in shear with either clamped edges (see ref. 2) or simply supported edges (see ref. 3 or ref. 4, p. 384) but nothing is available for orthotropic plates with edge-support conditions falling between these limits, the range in which most practical corrugated webs will fall. The use of charts for simply supported shear webs will

predict buckling at unduly small loads in most practical applications. The amplitude of corrugations in corrugated webs is relatively large compared with the thickness of a conventional plate with the same bending stiffness. Thus, there is a greater opportunity for restraining the rotational deformation along the edges of the corrugated webs. On the other hand, the edge support is not likely to be such that deformations are completely restrained in any practical application. Hence, design information for webs in which the rotational deformations along the edges of the web are only partially restrained is needed.

Design information is also needed regarding the effect of restrained warping on the buckling load of corrugated webs. The only information available on this effect is in reference 5, where buckling loads are given for long clamped corrugated webs with complete restraint against warping along the edges. The calculations were made for a specific corrugation shape (square wave) and indicate that the effect of restrained warping on buckling may be considerable. This effect is neglected in usual orthotropic plate analyses of corrugated webs.

The present paper extends previous calculations to include edge support conditions between clamped and simply supported edges for orthotropic shear webs with geometric properties characteristic of corrugated webs. The effect of restrained warping on buckling is taken into account in an approximate manner by an extension of the work of reference 5. In addition, the results of some tests on corrugated shear webs are presented and discussed.

SYMBOLS

D_1 plate flexural stiffness in longitudinal direction, $\approx \frac{t}{\bar{t}} \frac{Et^3}{12}$, in-kips

D_2 plate flexural stiffness in depthwise direction, $\approx E\bar{t}\rho^2$, in-kips

D_{12} plate stiffness, $\frac{\mu_x D_2 + \mu_y D_1 + 2D_{xy}}{2}$, in-kips

D_{xy} plate twisting stiffness, in-kips

E Young's modulus, ksi

M moment per inch of length of plate, kips

N_{xy} shear load per inch of plate, kips/in.

P beam load at web failure, kips

S shear load in web, kips

b effective depth of corrugated web between attachment members, in.

d amplitude of corrugations in corrugated plate, in. (fig. 4)

f effective rivet offset, in. (fig. 10)

g attachment angle dimension, in. (fig. 10)

h shear-beam depth measured between centroid of compression cover and centroid of tension cover, in.

k_S shear buckling coefficient, $\frac{N_{xy} b^2}{4\sqrt[4]{D_1 D_2^3}}$

l unsupported length of web between end buffer bays, in.

p pitch of corrugations in plate, in. (fig. 4)

t thickness of sheet in corrugated plate, in.

$\bar{t}$ area per inch of corrugated plate expressed as equivalent sheet thickness, in.

t_A thickness of attachment angle, in. (fig. 10)

w plate deflection, in.

x,y coordinates measured along and depthwise of web, in.

γ shear strain

Γ bending-torsion constant of corrugated plate, $in.^5$

δ lateral deflection of web, in.

ϵ restraint parameter, $\frac{M}{\theta} \frac{b}{D_2}$

θ edge rotation of web, radians

λ wave length, in.

μ Poisson's ratio

μ_x, μ_y Poisson's ratio associated with bending of corrugated plate in x- and y-directions. The product $\mu_x \mu_y$ is taken to be zero in this paper.

ρ radius of gyration of corrugated plate about centroidal axis, in.

τ shear stress, ksi

$\bar{\tau}$ efficiency parameter, ksi (eq. (12))

Subscripts:

av average

cr critical

e edge

eff effective

el elastic limit

max maximum

CALCULATIONS

The differential equation employed in the calculations was taken from reference 5. In the notation of the present paper, it is

$$D_1 \frac{\partial^4 w}{\partial x^4} + 2D_{12} \frac{\partial^4 w}{\partial x^2 \partial y^2} + D_2 \frac{\partial^4 w}{\partial y^4} - E\Gamma \frac{\partial^6 w}{\partial x^2 \partial y^4} + 2N_{xy} \frac{\partial^2 w}{\partial x \partial y} = 0 \qquad (1)$$

This equation is the usual differential equation expressing the equilibrium of elements of an orthotropic plate buckled in shear (see ref. 4,

p. 380) except for the $\frac{\partial w^6}{\partial x^2 \partial y^4}$ term which has been added to account for the fact that the effective twisting stiffness of corrugated sheet is highly influenced by the restraint of in-plane warping deformations. In this respect, the twisting of a corrugated sheet may be likened to that of an open section; that is, most of its stiffness is attributable to in-plane bending (so-called "bending stresses due to torsion") and the associated shear stresses. The use of equation (1) without the $\frac{\partial w^6}{\partial x^2 \partial y^4}$ term neglects this important property of corrugated sheet and may result in predicted buckling loads which are considerably lower than those obtained experimentally.

The number of calculations required is considerably reduced by taking advantage of two fundamental characteristics of corrugated sheet. The first characteristic is the large disparity between the magnitudes of the transverse and longitudinal bending stiffnesses of the plate. The result of the disparity is that the shear buckles are short in the longitudinal direction and even relatively short shear webs may be considered infinitely long for analysis purposes. The governing parameter in this case is $\frac{\lambda}{b}\sqrt[4]{\frac{D_2}{D_1}}$, which has values near unity. The stiffness D_2 is usually at least two or three orders of magnitude greater than D_1; hence, the quantity $\frac{\lambda}{b}$ is small.

The second characteristic is associated with the small twisting stiffness of corrugated sheet. For practical purposes the stiffness parameter $\frac{D_{12}}{\sqrt{D_1 D_2}}$ is so small that it can be taken to be zero with negligible error. The effect of this simplification is indicated in figure 1, where the buckling coefficient is plotted against $\frac{D_{12}}{\sqrt{D_1 D_2}}$. Values of the parameter $\frac{D_{12}}{\sqrt{D_1 D_2}}$ are generally less than 0.05 for the types of corrugations of current interest in structural applications. The curve shown was computed for clamped-edge conditions ($\epsilon = \infty$) but applies with negligible error to webs with other values of the edge-restraint parameter ϵ.

A solution to equation (1) can be obtained in the same manner as that employed in references 6 and 7 for shear buckling of isotropic

plates. The same stability equation applies in this case if the same boundary conditions are employed, that is, if plates with edges elastically restrained against rotational deformations are considered. The stability equation is given by

$$2\alpha\beta\left(4\gamma^2 - \frac{\epsilon^2}{4}\right)(\cosh 2\alpha \cos 2\beta - \cos 4\gamma) + \left[4\gamma^2(\alpha^2 - \beta^2) + (\alpha^2 + \beta^2)^2 + \left(4\gamma^2 + \alpha^2 - \beta^2\right)\frac{\epsilon^2}{4}\right]\sinh 2\alpha \sin 2\beta + \epsilon\left[\alpha\left(4\gamma^2 + \alpha^2 + \beta^2\right)\cosh 2\alpha \sin 2\beta + \beta\left(4\gamma^2 - \alpha^2 - \beta^2\right)\sinh 2\alpha \cos 2\beta - 4\alpha\beta\gamma \sin 4\gamma\right] = 0 \tag{2}$$

where

$$\epsilon = \frac{M}{\theta}\frac{b}{D_2} \tag{3}$$

and α, β, and γ for the case under consideration are given by the following relationships:

$$\left.\begin{aligned} \alpha^2 - \beta^2 - 2\gamma^2 &= \frac{2\chi\psi^2}{\zeta} \\ \gamma(\alpha^2 + \beta^2) &= k_S\frac{\psi}{\zeta} \\ (\alpha^2 + \gamma^2)(\beta^2 - \gamma^2) &= -\frac{\psi^4}{\zeta} \end{aligned}\right\} \tag{4}$$

where

$$\left.\begin{aligned} \chi &= \frac{D_{12}}{\sqrt{D_1 D_2}} \\ \psi &= \sqrt[4]{\frac{D_1}{D_2}}\frac{\pi b}{2\lambda} \\ \zeta &= 1 + \frac{4E\Gamma}{b^2\sqrt{D_1 D_2}}\sqrt{\frac{D_1}{D_2}}\left(\frac{\pi b}{2\lambda}\right)^2 \end{aligned}\right\} \tag{5}$$

and

$$k_S = \frac{N_{xy} b^2}{\sqrt[4]{D_1 D_2^3}} \tag{6}$$

The notation of references 6 and 7 is retained here in writing equation (2). The symbol γ should not be confused with shear strain, which is denoted by γ in other sections of this paper.

The first and last of relationships (4) can be solved for α and β to obtain

$$\left.\begin{aligned} \alpha &= \sqrt{\gamma^2 + \frac{\chi\psi^2}{\zeta} + 2\sqrt{\gamma^4 + \frac{\chi\psi^2}{\zeta}\gamma^2 + \frac{1}{4\zeta}\left(\frac{\chi^2}{\zeta} - 1\right)\psi^4}} \\ \beta &= \sqrt{-\gamma^2 - \frac{\chi\psi^2}{\zeta} + 2\sqrt{\gamma^4 + \frac{\chi\psi^2}{\zeta}\gamma^2 + \frac{1}{4\zeta}\left(\frac{\chi^2}{\zeta} - 1\right)\psi^4}} \end{aligned}\right\} \tag{7}$$

and the second of relationships (4) yields

$$k_S = \gamma(\alpha^2 + \beta^2)\frac{\zeta}{\psi} \tag{8}$$

Values of k_S can be determined from equations (2), (7), and (8) as follows: For selected values of ψ and ϵ, a value of γ is assumed and corresponding values of α and β are computed from equation (7). Values of α, β, and γ, together with the selected value of ϵ, are then substituted into the stability equation (2). If equation (2) is not satisfied, a new value of γ is assumed and the process repeated until a consistent set of values of α, β, and γ are found which satisfy equation (2). Then a value of k_S is computed from equation (8).

Calculated values of k_S $\left(\text{or } \frac{N_{xy} b^2}{\sqrt[4]{D_1 D_2^3}}\right)$ are plotted in figure 2 against $\frac{\lambda}{b}\sqrt[4]{\frac{D_2}{D_1}}$ for various values of the restraint parameter ϵ. In

constructing this figure, the parameter $\frac{D_{12}}{\sqrt{D_1 D_2}}$ was taken to be zero, as discussed earlier. Furthermore, the bending-torsion parameter $\frac{4E\Gamma}{b^2\sqrt{D_1 D_2}}$ was taken to be zero. The edge-restraint parameter was varied from the simple support value ($\epsilon = 0$) to the clamped value ($\epsilon = \infty$). This parameter is proportional to the rotational stiffness M/θ of each of the two cap members, and for calculation purposes was assumed to have the same value for each member. In many applications the cap members will differ or will have different stiffnesses because of stress conditions which differ. For these cases the buckling load, in order to be conservative, should be calculated by using properties of the cap member with the smallest stiffness.

Figure 3 shows the effect on buckling coefficient of changes in the bending-torsion parameter $\frac{4E\Gamma}{b^2\sqrt{D_1 D_2}}$ for both clamped and simply supported edge conditions. Considerable increases in k_s are indicated with increases in the bending-torsion parameter, particularly for clamped edges. The imposed boundary conditions are such that for simply supported edges ($\epsilon = 0$) in-plane warping along the edges of the plate is unrestrained, and for clamped edges ($\epsilon = \infty$) in-plane warping is fully restrained. Hence, for the $\epsilon = 0$ curve the increase in k_s is associated with restrained warping within the plate due to variable torque, whereas for the $\epsilon = \infty$ curve the increase in k_s is attributable to both restrained warping within the plate from variable torque and restrained warping at the edges of the plate.

Corresponding curves for other values of ϵ are not given in figure 3 because in any practical application the effect of restraining both edge rotations and warping cannot be handled with a single-restraint coefficient. A practical way for handling such a case might be to try to account for the restraint of edge rotations by proper calculation and then estimate the effect of restrained warping from figure 3. The correct value of k_s should lie between the two curves of figure 3; where between the curves is not known. It is known, however, that edge warping deformations are extremely difficult to prevent, and therefore the condition of complete restraint ($\epsilon = \infty$) is not likely to be approached in corrugated shear webs of conventional design. On the other hand, edge conditions may be such that some restraint is provided which cannot be properly accounted for with the use of figure 3. It is expected, however, that this effect will generally be small and that the

conservative assumption of unrestrained warping along the supported edges should suffice in most cases. Figures 2 and 3 will be used later in assessing the behavior of some tests on corrugated shear webs.

TESTS

Shear tests were conducted on seven beams with corrugated webs in order to obtain information regarding the buckling strength of such structures. The beams were of built-up construction and differed from one another only in depth.

Test Beams

Details of construction of the test beams are given in figure 4 and table I. The web corrugations were composed of angular waves formed by a series of straight equal-length segments. The particular orientation of the segments was selected on the basis of an elastic weight-strength analysis of such corrugations in which the angle between adjoining segments was allowed to vary. Accordingly, the beams in this series of tests include proportions of nearly optimum design.

The test beams were constructed with short buffer bays at either end to facilitate the introduction of load into the specimen in a uniform manner. The buffer bays must be short for this purpose because, as discussed earlier, the buckles tend to be short in the length direction. In a preliminary test of a beam with somewhat longer buffer bays than those finally used for the test specimens, buckling was observed to occur in the buffer bay at a load of approximately 70 percent of that computed for the test section.

Reinforcement strips were used at the top and bottom of the webs of the test beams to delay local buckling. Use of the strips was suggested by a preliminary test also. The design was such that local buckling of the elements of the corrugation was expected to occur at about the same stress level as buckling of the corrugated web as an orthotropic plate. However, local buckling of the flat elements occurred earlier than expected. The buckles seemed to emanate from the unsupported ends of the elements of the corrugations that were not attached to the web-attachment angles at a stress of approximately 85 percent of the buckling stress computed for the elements on the basis of simple support all around. The premature buckling triggered web instability soon thereafter. Consequently, 1-inch-wide strips of the same thickness as the web were bonded to the web of the test beams at the top and bottom to provide support to the otherwise free edges.

The strips have the additional advantage of alleviating the complexity of the problem of providing an adequate attachment between the web and the web-attachment angles; this problem arises because attachments to the web can be made only at the crests of the corrugations. The strips have the disadvantage of adding weight.

The webs of the beams were fastened at each wave crest to the web-attachment angles with three conventional rivets (see figs. 4(c) and 4(d)). The geometry was such that the attachment angles did not have to be scalloped, as is often done. The edge reinforcing strips, which are nominally 1/8 inch deeper than the attachment leg of the web-attachment angle, are visible in figure 4(d) for beams 6 and 7. They are on the other side of the web of beam 5. The light areas at the tops and bottoms of the webs are areas which were chemically cleaned during fabrication for bonding the strips to the web.

The specimens were constructed of 7075-T6 aluminum alloy. Typical material properties were used in reducing the data. Young's modulus E was taken as 10,500 ksi, and Poisson's ratio μ was assumed to be 0.32.

Procedure

The test beams were cantilevered to a heavy backstop and loaded at the tip with a vertically applied load (see fig. 5). The load was applied in small increments, and between load increments the webs were examined for evidence of buckling.

To help further in detecting buckling, particularly local buckling of the flat-plate elements of the corrugations, strain measurements were taken on the webs of the beams. The strains were autographically recorded during the tests. Also, in the early tests buckle bars were used to help detect buckling of the corrugated sheet as an orthotropic plate. A buckle bar was mounted on each side of the web and rested on the web. Any lateral movement of the bar resulting from web buckling excited a strain gage whose output was autographically recorded during the test. For the tests of beams 5 to 7, the buckle bar on either side of the web was replaced with two banks of three dial gages. The dial gages were read between load increments and were removed prior to expected failure.

Results

The shear loads supported by the test beams at failure are given in table I. The average shear stresses in the webs at failure computed according to the formula

$$\tau = \frac{P}{ht} \tag{9}$$

are also given. The shear stress in the webs at failure as deduced from strain-gage readings near the neutral axis of the beams was usually about 5 percent less than the shear stresses computed according to formula (9), and in the case of beam 4 was 10 percent less. This discrepancy, which was greater at high loads than at low loads, is believed to be the result of some out-of-plane (buckling) deformations of the webs even at relatively low loads. The shear distribution in a buckled shear web is not uniform; the areas near the flanges carry more than their proportionate share. Very little of the discrepancy can be attributed to the so-called "portal-frame action." Reference 8 was used to estimate the load carried by the portal frame of the test beams, and it was found to be less than 1 percent of that carried by the web in every instance.

Lateral deflections of the webs, measured with dial gages, are plotted in figure 6 as a function of applied load. No definite buckling loads are indicated by the curves. Lateral deflections evidently started to grow from the beginning of load application, and at the predicted critical load for the webs (denoted by tick marks on the curves) had grown to approximately 2 percent of the web thickness d. The calculation of the critical loads will be discussed subsequently. Observation of the webs during loading indicated that the buckles did not become readily visible until just prior to failure, when a well-defined buckle pattern could usually be observed. This behavior suggests that buckled shear webs are rather stable, and agrees with previous calculations and observations. References 9 to 11 show that the postbuckling behavior of noncorrugated webs, as determined by the load-shortening characteristics of the web, depends strongly upon boundary conditions and is characterized by a rather mild digression from the prebuckling loading path compared with that of more familiar flat or curved plates in compression. The semiempirical method of reference 8 is in agreement with references 9 to 11 in this respect. The digression would, of course, become more pronounced when the influence of the buckles in creating a nonuniform stress distribution caused inelastic stresses in the web. The inelastic stresses would intensify buckle growth, which would cause larger plastic stresses and eventually cause web failure. Failure of the webs of the test beams is believed to have occurred in this manner.

DISCUSSION

Values of shear stress at beam failure are plotted in figure 7 against the computed critical shear stress for the beams. The critical

shear stress was computed with the use of figures 2 and 3. The edge restraint offered the web by the cap and web-attachment angles (ϵ of fig. 2) was computed in accordance with the appendix of this paper, and the bending-torsion constant (Γ of fig. 3) was taken from figure 8, which gives values of the bending-torsion constant for three common types of corrugations. The curves of figure 8 were computed by the procedure used in reference 5 for square-wave corrugations.

In applying figure 3 to the present test beams, the in-plane warping was assumed to be unrestrained along the edges of the webs. This assumption is undoubtedly conservative, because the doubler strips along the edges of the web provide some restraint to in-plane warping. Connections between the web and the attachment angles occurred only near points of zero warping. Hence, the attachment angles and cap member were probably not very instrumental in restraining warping. The web depth b was taken as the distance between the centers of clusters of rivets fastening the webs to the web-attachment angles at the tops and bottoms of the webs. This value of depth would seem to be reasonable for beams (such as the test beams) in which the caps and web-attachment angles are so heavy that bending deformations of the web at the lines of attachment are nearly prevented. It may not be as reasonable for beams with much lighter web-attachment angles than those used in the test beams. The shear stresses computed with the use of figures 2 and 3 were corrected for plasticity effects by using the method of reference 12 and a compression stress-strain curve with a proportional-limit stress of 55 ksi and a 0.2-percent-offset yield stress of 72 ksi.

The deeper webs of figure 7 (those with small values of critical stress) took considerably more stress at failure than the computed critical shear stress. However, the shear stress at failure for the two shallower webs agrees well with computation. The shear stress of the shallowest agrees well with the calculation for local buckling of the flat elements of the corrugations with the elements assumed to be simply supported all around (the horizontal curve), and the shear stress of the other agrees well with the computed buckling stress of the web as an orthotropic plate (the 45° curve).

The trend of the data for the deeper beams follows generally that of the curve labeled τ_{av}. This curve was computed from the formula

$$\tau_{av} = \tau_{el}^{2/3} \tau_{cr}^{1/3} \qquad (10)$$

The formula was suggested by the behavior of the beams as discussed earlier. It gives the average shear stress τ_{av} in a buckled web at failure when the maximum shear stress (so-called "edge shear stress")

is the elastic limit stress τ_{el} of the web material and when the "load shortening" curve for the web can be approximated by the relationship (see refs. 13 and 14)

$$\frac{\tau_{av}}{\tau_e} = \left(\frac{\gamma_{cr}}{\gamma_e}\right)^{1-m} \tag{11}$$

The exponent m, which denotes the ratio of the slope of the load-shortening curve immediately following buckling to the slope of the curve preceding buckling, was taken to be 2/3.

The assumptions expressed and implied in the use of equation (10) are many, and their validity has not been verified; the equation is not given as a design formula, but as an aid in interpreting the test results.

The test results are given in figure 9 on a structural efficiency plot of $\bar{\tau}$ against structural index. The ordinate $\bar{\tau}$ is a fictitious shear stress given by the equation

$$\bar{\tau} = \frac{S}{h\bar{t}_w} \tag{12}$$

where $\bar{t}_w$ is the average weight of the web per unit area divided by the density of the web material. In computing $\bar{t}_w$, the weight of the doubler strips was included as part of the weight of the shear webs. However, the weight of web-attachment angles and cap members was not included. These members should be considered a part of the material which carries bending loads in weight-strength analyses unless the members function only as fastening members (such as the scalloped legs of web-attachment angles in beams where legs of the web-attachment angles are scalloped in order to facilitate fabrication) and do not carry bending loads.

Also shown in figure 9 is a curve for 7075-T6 aluminum-alloy diagonal-tension webs that was taken from reference 8, and a curve for the corrugated-web beams based on buckling calculations in which average geometric properties were used for the seven beams under consideration. The break in the computed curve corresponds to the transition from buckling of the corrugated web as an orthotropic plate to buckling of the flat elements of the corrugations (local buckling). This point evidently corresponds to the web of optimum depth among those webs considered. Calculations and experiment are in reasonable agreement for this web. (see fig. 7). Hence, the buckling calculations used herein would seem

to be adequate for making weight-strength predictions for the value of structural index of concern here $\left(\frac{S}{h^2} = 0.05 \text{ ksi}\right)$. Similar buckling calculations should be adequate for making weight-strength predictions for values of structural index greater than 0.05 ksi. Webs of optimum design in this range experience more plasticity at buckling than the webs just discussed. Hence, a buckling analysis should again be adequate for predicting failing loads. The validity of using the buckling analysis for predicting the failing loads of beams of optimum design in the region to the left of $\frac{S}{h^2} = 0.05$ in figure 9 cannot be verified with the present tests, although it would seem that the calculations should be adequate at least for values of structural index not far removed from 0.05. The optimum web is so proportioned that local buckling of the flat elements of the corrugation and buckling of the corrugated web as an orthotropic plate occur simultaneously. Either of the buckling modes occurring alone at low stress levels would not be expected to precipitate failure until the web was loaded substantially beyond the computed buckling load. However, both modes occurring simultaneously at low stress levels may trigger failure, as discussed earlier in connection with a preliminary test of a beam.

Figure 9 indicates that corrugated shear webs are somewhat lighter than diagonal-tension webs in the range of structural indices considered. The corrugated shear web is also somewhat stiffer than the diagonal-tension web. For instance, the corrugated web of figure 9 at a structural index of 0.05 ksi has an effective shear stiffness of about 80 percent of that of an equivalent-weight unbuckled flat plate, whereas the corresponding diagonal-tension web is highly buckled and has an effective stiffness of 50 to 60 percent of that of the unbuckled flat plate. Furthermore, the corrugated web has a greater resistance to crushing than the diagonal-tension web. The complete structure, in the case of the corrugated web, is effective in restraining crushing loads, whereas only the uprights on a diagonal-tension web are very effective. On the other hand, the corrugated web is more difficult to fabricate and hence is more costly.

CONCLUDING REMARKS

The results of calculations and tests to determine the buckling strength of corrugated shear webs are presented and discussed. The charts presented enable the designer to compute readily the small-deflection shear buckling stress for webs, including the effect of restraint of warping. The tests indicate that the most attractive webs

from a weight-strength point of view are those of balanced design; that is, with local buckling of the flat elements of the corrugations in the web balanced against general buckling of the web as an orthotropic plate. In the tests reported, the beams of nearly optimum design had buckling stresses just slightly greater than the proportional-limit stress of the web material. Hence, as might be expected, the buckling charts could be used to predict the failing strength of the beams with good accuracy. The beams of unbalanced design took more load than their predicted buckling load before failing.

Langley Research Center,
National Aeronautics and Space Administration,
Langley Field, Va., April 21, 1960.

APPENDIX

EDGE RESTRAINT OF TEST WEBS

The chart of figure 2 is not readily applicable to the tests reported herein without additional information regarding (1) the elastic restraint offered the web by the attachment between the web and the cap member and (2) the elastic restraint offered the web by the cap members. The stiffness of each of these may be considered separately and the effective stiffness computed as

$$\frac{1}{M/\theta} = \frac{1}{M/\theta_1} + \frac{1}{M/\theta_2} \qquad (A1)$$

The stiffness parameter can then be computed from formula (3). The stiffness M/θ_1 is the stiffness computed on the assumption that the cap member is rigid (that is, it does not deform under load), and M/θ_2 is the stiffness computed on the assumption that the web-attachment angles are rigid.

The Stiffness M/θ_1

The stiffness M/θ_1 is associated with cross-sectional deformations of the web-attachment angles under the action of a sinusoidally distributed torque loading as depicted in figure 10(a). The deformation of the cap member is neglected in computing the deformations. The deformations of rivets and bolts as well as the local deformations of the corrugated sheet in the vicinity of the rivets or bolts should be considered. This, of course, would involve rather lengthy and somewhat involved calculations if an accurate evaluation were attempted. Instead, a semiempirical treatment which was found to work well in analyzing the deformations of attachments in multiweb beams and stiffened panels will be used (see refs. 15 and 16).

The deformation of the web-attachment angles is assumed to be as depicted in figure 10(b). One leg of the attachment angle is assumed to become tangent to (effectively clamped to) the cap member at a distance f from the center line of the other leg, which is assumed to be pin-connected to the web at the bolt or rivet connection. The other attachment angle is neglected in the computation, and the web is assumed

to rotate about an edge of the corrugation, as shown. With these assumptions and the additional assumption that the buckle length is large compared with the width of leg of the attachment angle, the stiffness can be written as

$$\frac{M}{\theta_1} = \frac{E\left(d + \frac{t_A}{2}\right)^2}{\left(\frac{f}{t_A}\right)^3}\left(\frac{1 + 3\frac{f}{g}}{4 + 3\frac{f}{g}}\right) \qquad \text{(A2)}$$

It will be noted that under the assumptions made, the stiffness M/θ_1 is independent of wavelength. Formula (A2) is written for the case of web-attachment angles that are not scalloped. When the web-attachment angles are scalloped, the $3\frac{f}{g}$ terms should be replaced by $3\frac{f}{g}\frac{EI_{eff}}{EI}$ where EI_{eff} is the bending stiffness of the scalloped leg of the angle and EI is the bending stiffness of the leg without scalloping.

The Stiffness M/θ_2

The stiffness M/θ_2 is given in figure 11 in terms of the dimensions of the cap member. This stiffness is directly related to the stiffness S^{III} of reference 17, and figure 11 was prepared from the tabulated data of that reference. The stiffness M/θ_2 is a function of the buckle length λ.

REFERENCES

1. Seydel, Edgar: Schubknickversuche mit Wellblechtafeln. Jahrb. 1931 der DVL E. V. (Berlin-Aldershof), pp. 233-245.

2. Smith, R. C. T.: The Buckling of Plywood Plates in Shear. Rep. ACA-29, Australian Council for Aero., Oct. 1946.

3. Seydel, Edgar: The Critical Shear Load of Rectangular Plates. NACA TM 705, 1933.

4. Timoshenko, S.: Theory of Elastic Stability. McGraw-Hill Book Co., Inc., 1936.

5. Smith, Geoffrey E.: Elastic Buckling in Shear of Infinitely Long Corrugated Plates With Clamped Parallel Edges. M.A.E. Thesis, Cornell Univ., 1957.

6. Stowell, Elbridge Z.: Critical Shear Stress of an Infinitely Long Flat Plate With Equal Elastic Restraints Against Rotation Along the Parallel Edges. NACA WR L-476, 1943. (Formerly NACA ARR 3K12.)

7. Stowell, Elbridge Z., and Schwartz, Edward B.: Critical Stress for an Infinitely Long Flat Plate With Elastically Restrained Edges Under Combined Shear and Direct Stress. NACA WR L-340, 1943. (Formerly NACA ARR 3K13.)

8. Kuhn, Paul, Peterson, James P., and Levin, L. Ross: A Summary of Diagonal Tension. Part I - Methods of Analysis. NACA TN 2661, 1952.

9. Kromm, A., and Marguerre, K.: Behavior of a Plate Strip Under Shear and Compressive Stresses Beyond the Buckling Limit. NACA TM 870, 1938.

10. Levy, Samuel, Fienup, Kenneth L., and Woolley, Ruth M.: Analysis of Square Shear Web Above Buckling Load. NACA TN 962, 1945.

11. Levy, Samuel, Woolley, Ruth M., and Corrick, Josephine N.: Analysis of Deep Rectangular Shear Web Above Buckling Load. NACA TN 1009, 1946.

12. Stowell, Elbridge Z.: Critical Shear Stress of an Infinitely Long Plate in the Plastic Region. NACA TN 1681, 1948.

13. Anderson, Roger A., and Anderson, Melvin S.: Correlation of Crippling Strength of Plate Structures With Material Properties. NACA TN 3600, 1956.

14. Zender, George W., and Hall, John B., Jr.: Combinations of Shear, Compressive Thermal, and Compressive Load Stresses for the Onset of Permanent Buckles in Plates. NASA TN D-384, 1960.

15. Semonian, Joseph W., and Anderson, Roger A.: An Analysis of the Stability and Ultimate Bending Strength of Multiweb Beams With Formed-Channel Webs. NACA TN 3232, 1954.

16. Semonian, Joseph W., and Peterson, James P.: An Analysis of the Stability and Ultimate Compressive Strength of Short Sheet-Stringer Panels With Special Reference to the Influence of the Riveted Connection Between Sheet and Stringer. NACA Rep. 1255, 1956. (Supersedes NACA TN 3431.)

17. Kroll, W. D.: Tables of Stiffness and Carry-Over Factor for Flat Rectangular Plates Under Compression. NACA WR L-398, 1943. (Formerly NACA ARR 3K27.)

TABLE I

DIMENSIONS OF TEST BEAMS AND RESULTS OF TESTS

Beam	t, in.	d, in.	h, in. (a)	l, in. (b)	$\frac{p}{d}$	$\frac{\rho}{d}$	$\frac{\bar{t}}{t}$	P, kips	τ, ksi
1	0.0255	0.744	16.3	34.4	3.70	0.408	1.31	14.6	35.2
2	.0248	.695	18.3	34.4	3.96	.408	1.26	14.9	32.9
3	.0241	.696	20.3	34.4	3.95	.408	1.26	14.2	29.1
4	.0248	.693	22.3	34.2	3.94	.408	1.26	16.9	30.6
5	.0239	.706	22.3	34.4	3.89	.408	1.26	15.2	28.5
6	.0239	.706	25.3	34.4	3.89	.408	1.26	16.3	27.0
7	.0242	.706	28.3	34.4	3.89	.408	1.26	17.0	24.8

[a]Beam depth measured between centroids of compression and tension cap members.

[b]Unsupported length of web between end buffer bays.

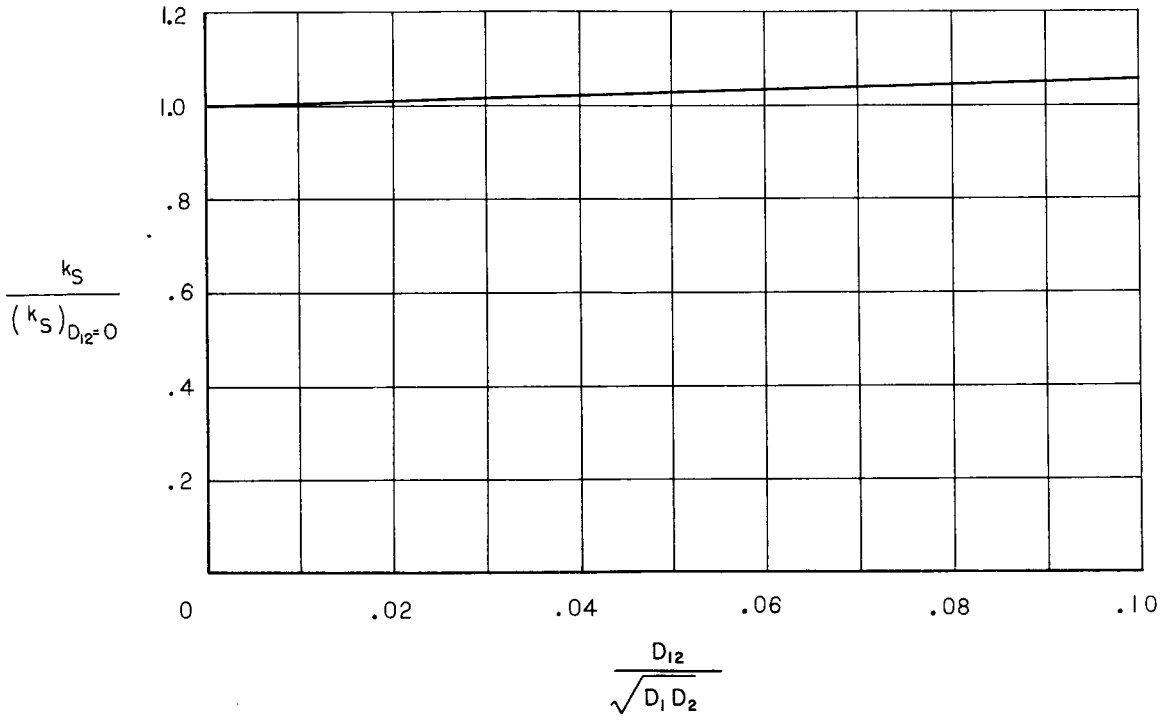

Figure 1.- Effect of twisting stiffness of orthotropic plates on buckling strength.

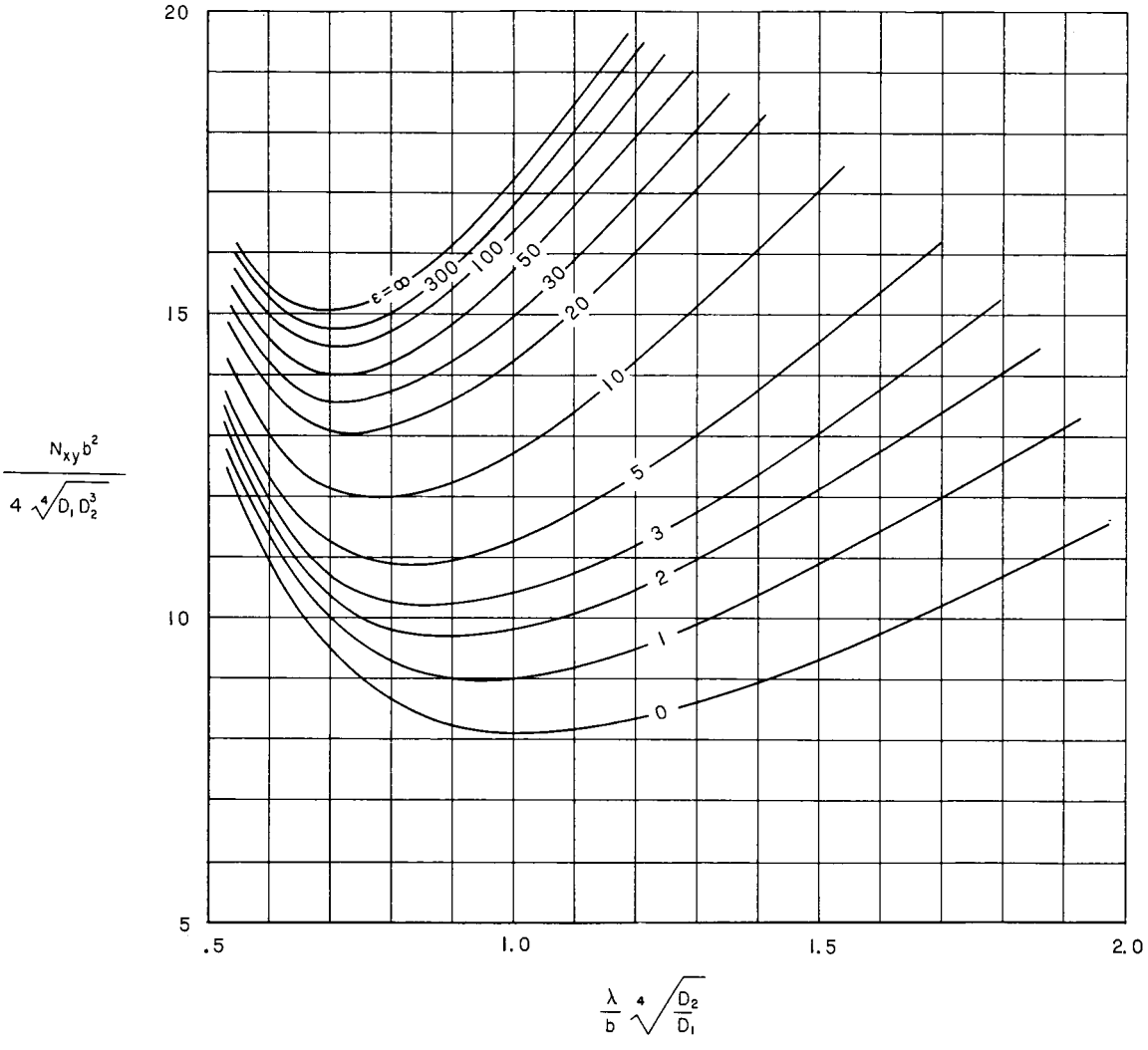

Figure 2.- Shear buckling coefficients of long corrugated plates with nondeflecting edge supports.

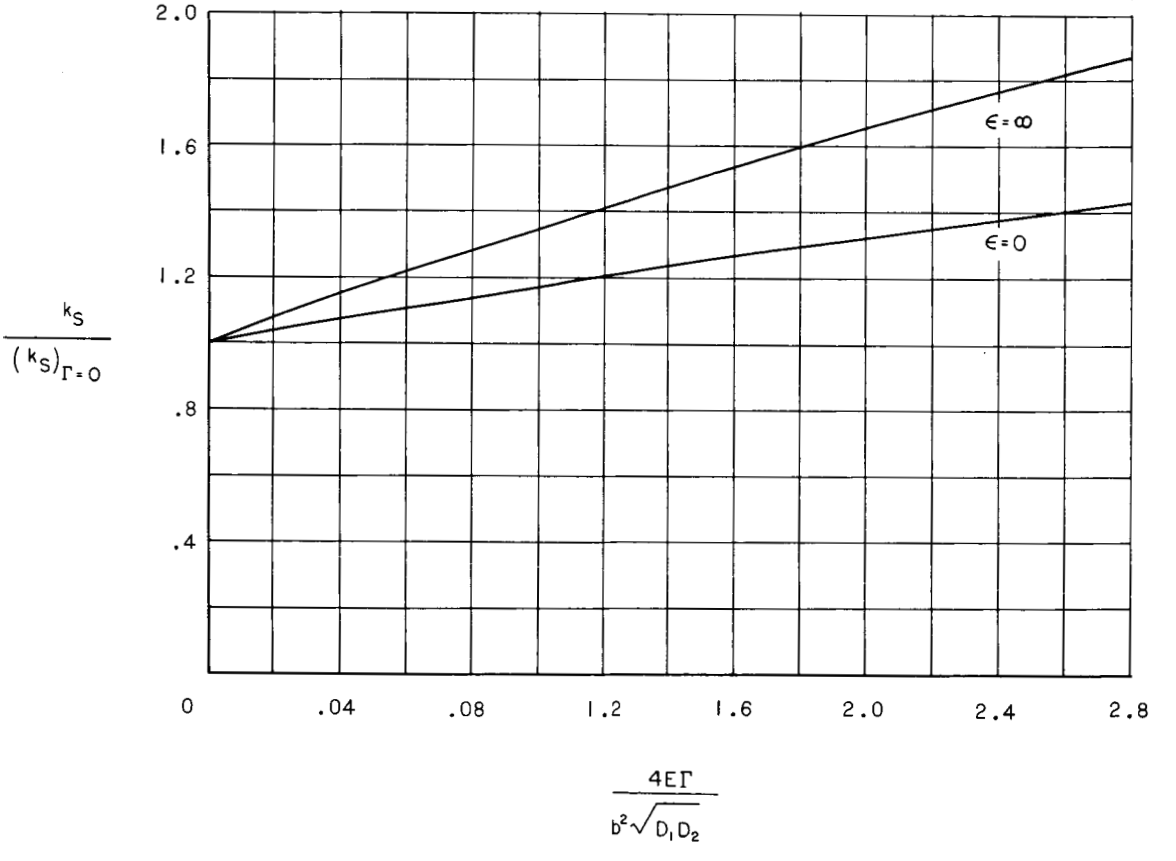

Figure 3.- The effect of restraint of warping on the buckling strength of corrugated plates in shear.

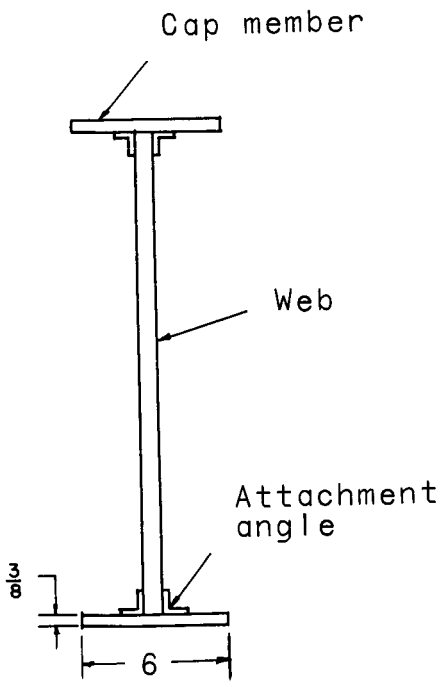

(a) Cross section of beam.

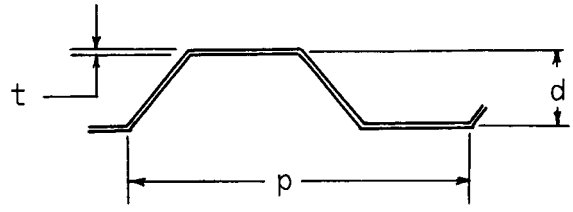

(b) Corrugation details.

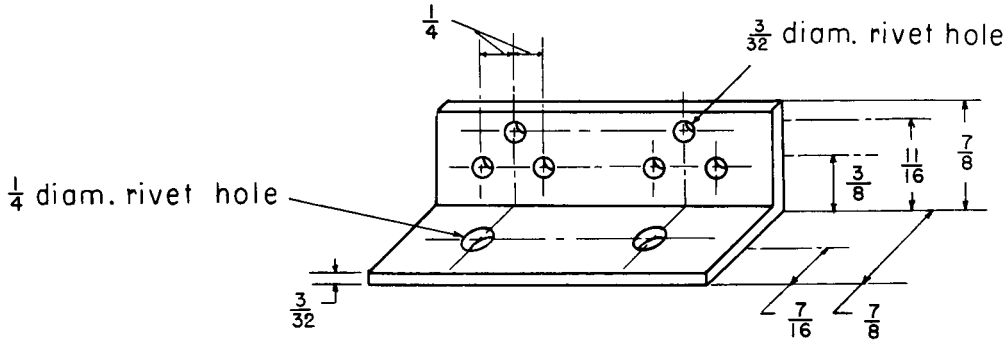

(c) Web-attachment-angle details.

Figure 4.- Details of test beams.

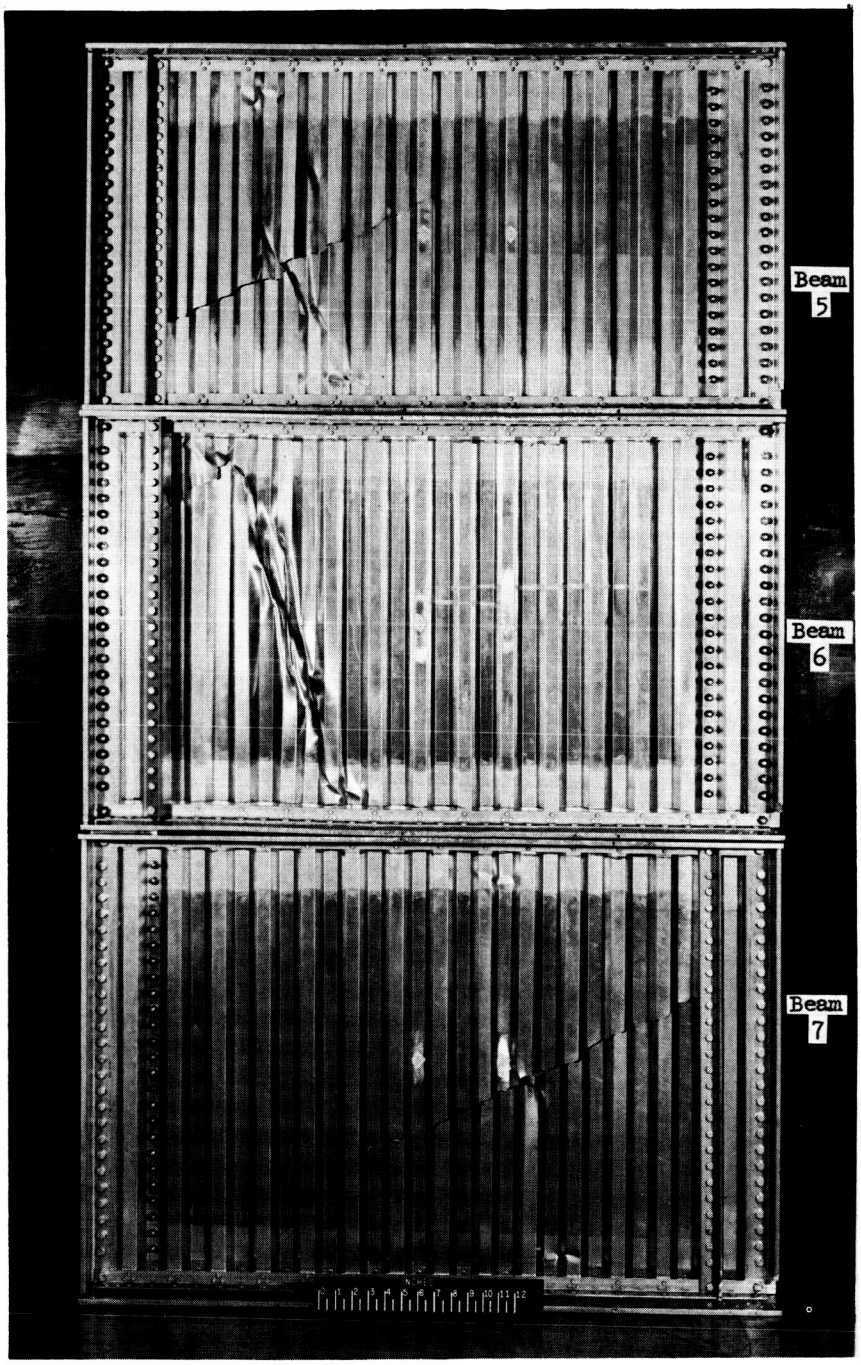

(d) Beams 5 to 7 after testing. L-59-7688.1

Figure 4.- Concluded.

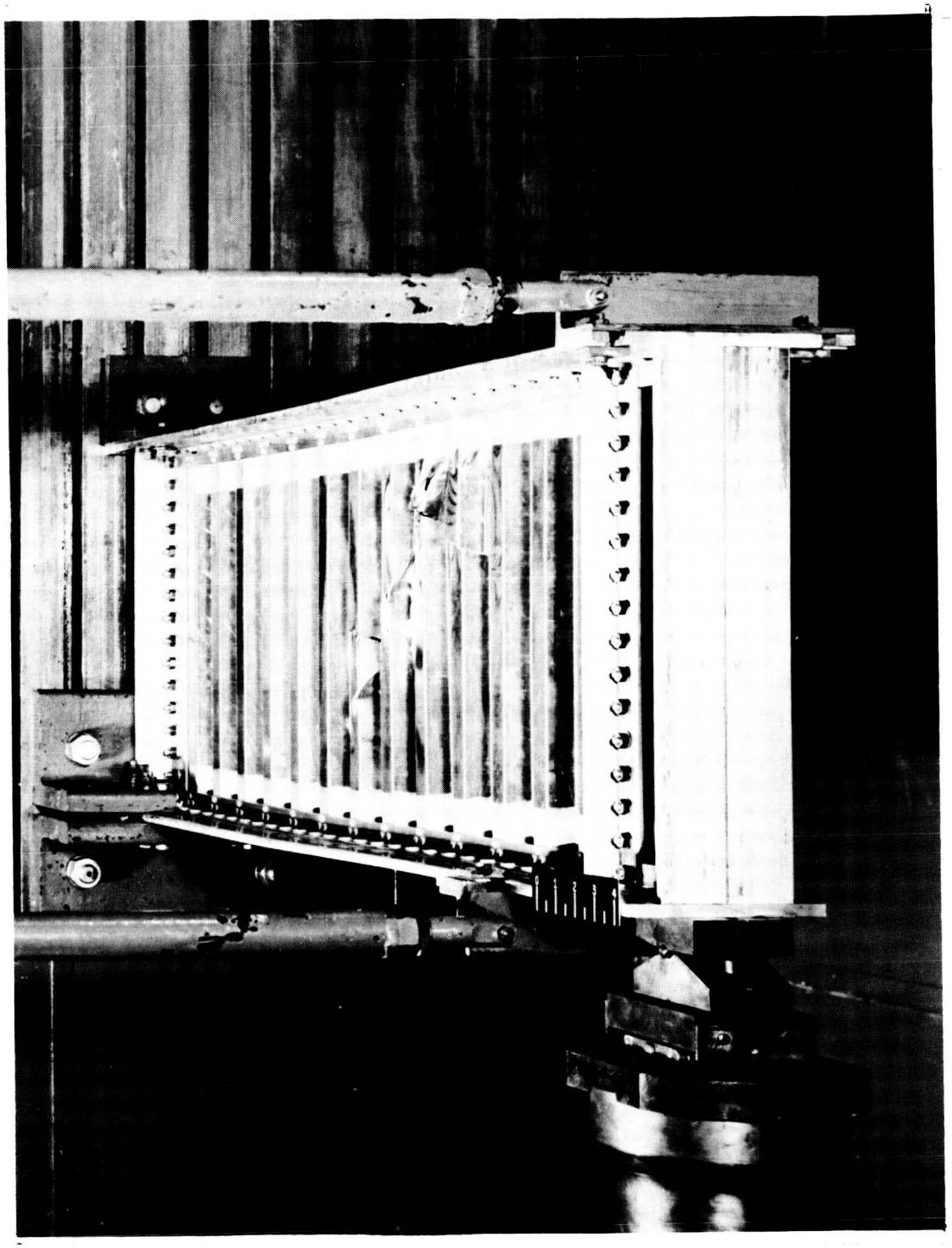

L-58-525

Figure 5.- Beam 1 after testing. Horizontal guide arms shown were used to eliminate the possibility of lateral instability failures.

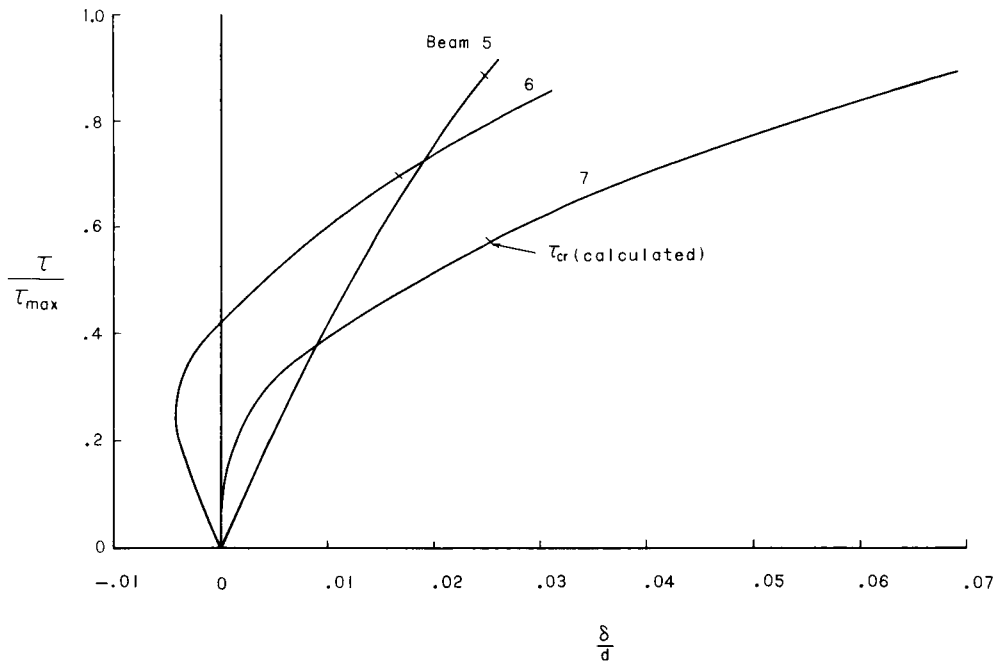

Figure 6.- Lateral deflection of webs of beams 5 to 7. Only the largest of the six measured deflections is shown.

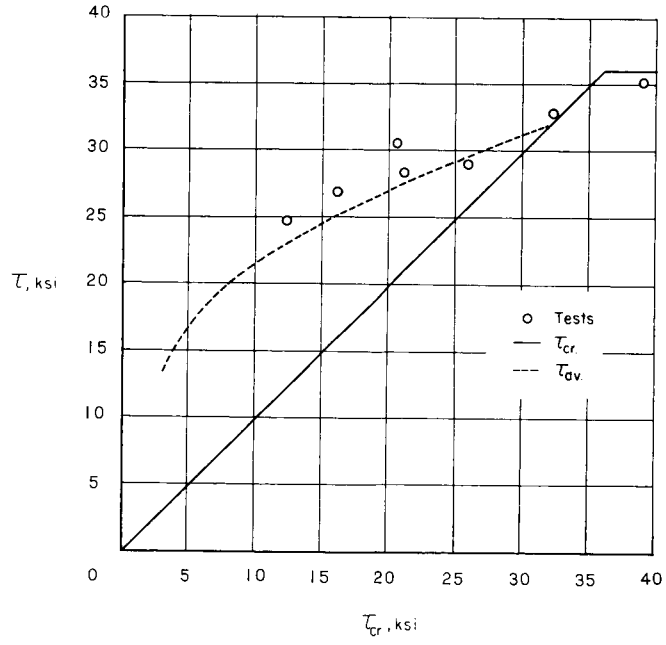

Figure 7.- Failing stress of test beams plotted against calculated buckling stress.

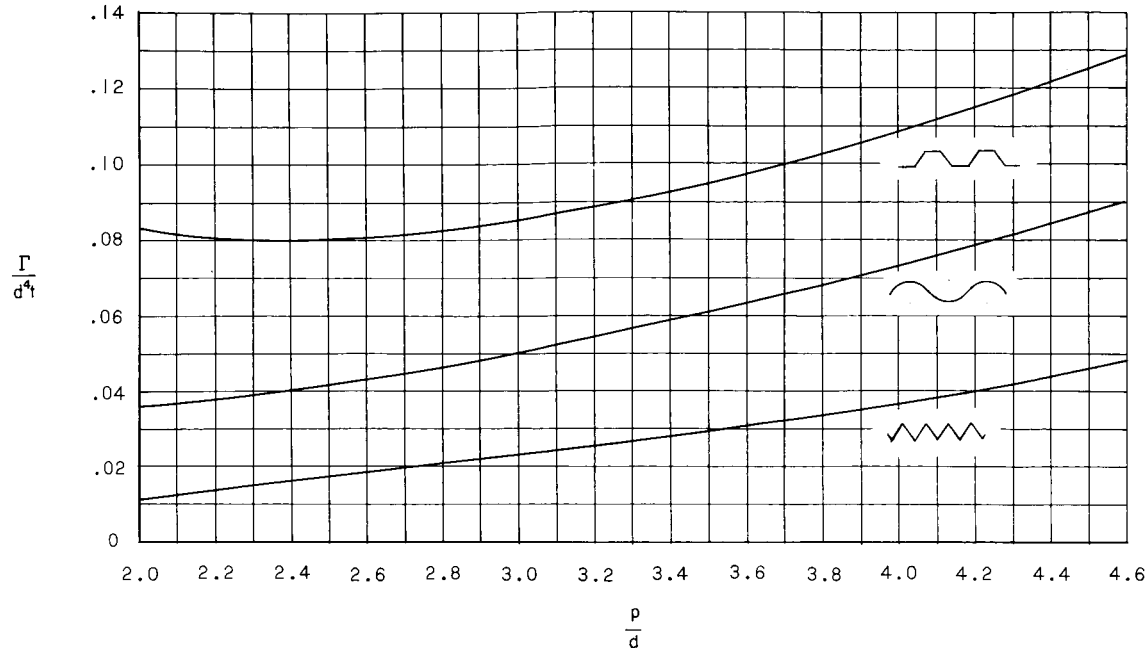

Figure 8.- Bending-torsion parameter for three common types of corrugations.

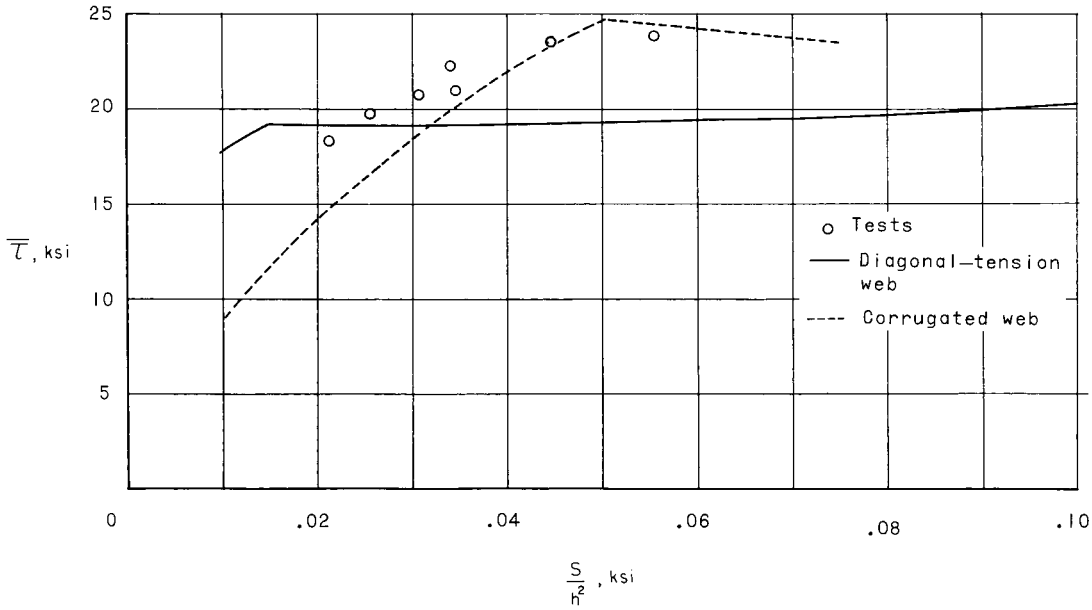

Figure 9.- Structural efficiency of test beams and comparison with diagonal-tension beams.

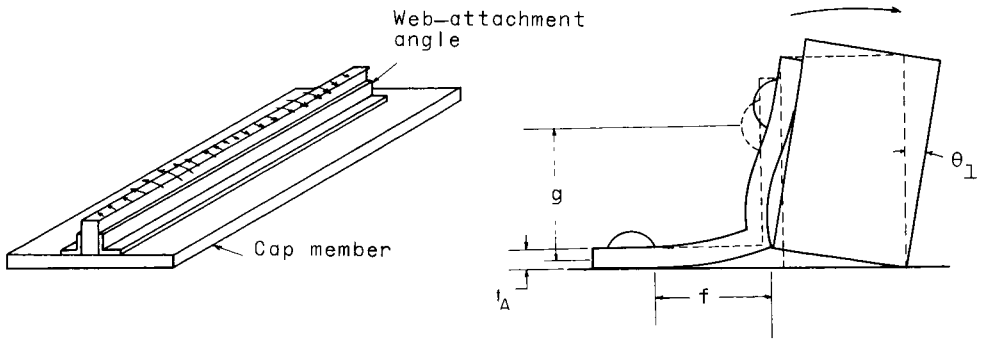

(a) Loads. (b) Deformations.

Figure 10.- Loads and deformations of web-attachment angles.

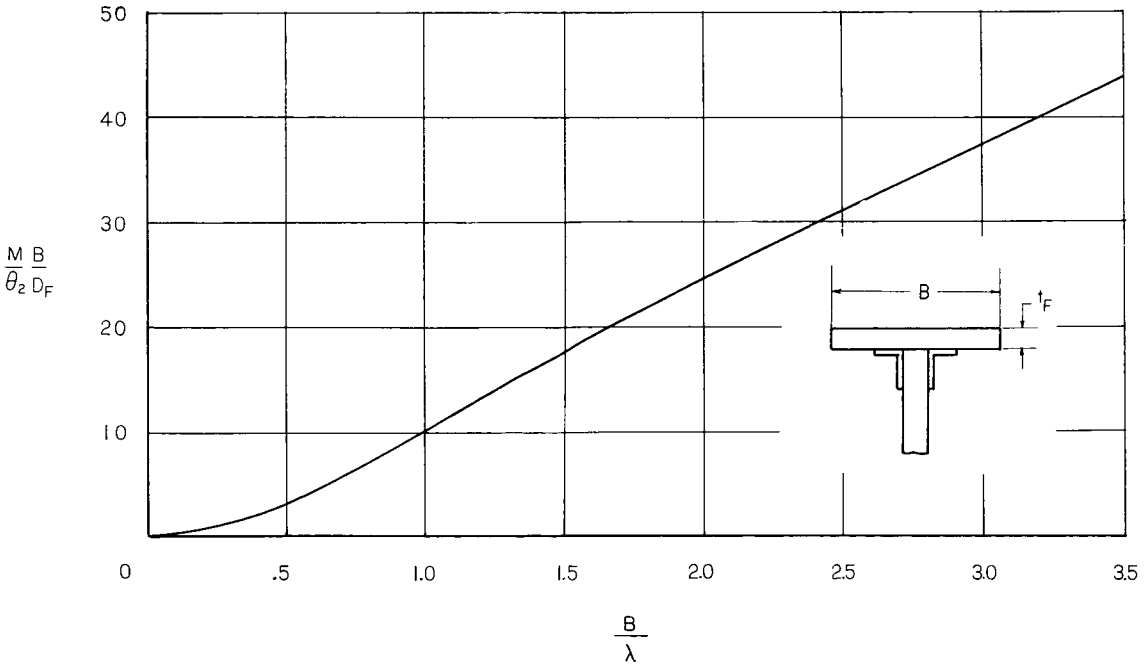

Figure 11.- Stiffness of cap member. The symbol D_F denotes bending stiffness of cap member $\left(D_F = \frac{Et_F^3}{12(1-\mu^2)}\right)$.